ARTICLE NO. 78-1080R

Vectoring Nonaxisymmetric Nozzle Jet Induced Effects on a V/STOL Fighter Model

W.C. Schnell* and R.L. Grossman†
Grumman Aerospace Corporation, Bethpage, N.Y.

An experimental program sponsored by the Air Force Flight Dynamics Laboratory, utilizing a 1/8th scale, advanced twin engine, thrust vectoring, V/STOL fighter wind-tunnel jet effects model developed for the Naval Air Propulsion Test Center, was completed in June 1977. The findings show significant aircraft performance improvements when the nonaxisymmetric nozzles are vectored.

I. Introduction

During the past several years, studies directed toward the investigation and evaluation of the nonaxisymmetric exhaust nozzle and its benefits and potential problem areas have been undertaken in considerable depth by both industry and government (Air Force, Navy and NASA). The results found from these recent studies, for both V/STOL and CTOL twin engine tactical fighters, are summarized in Refs. 1 and 2.

The objective of this experimental program consisted of three primary parts: 1) measurement of the static internal performance characteristics of several nonaxisymmetric nozzles and a baseline axisymmetric nozzle; 2) comparison of the installed dry power performance of the nonaxisymmetric nozzles with the axisymmetric nozzles; and 3) measurement of the inflight thrust vectoring propulsion induced aerodynamic effects of the augmented deflector exhaust nozzle (ADEN) installations. This paper describes the results from the third part of this program. In-depth discussion of the entire test results appears in an Air Force Flight Dynamics Laboratory report.[3]

II. Description of the ADEN Nonaxisymmetric Nozzle

The augmented deflector exhaust nozzle was developed by the General Electric Company for the United States Navy to meet requirements for an efficient, lightweight, thrust deflecting system to be used on supersonic V/STOL aircraft.

The ADEN V/STOL exhaust system (Fig. 1) is a variable area internal/external expansion type, nonaxisymmetric nozzle with throat area controlled by a variable geometry convergent-divergent upper flap assembly. The variable position ventral flap located downstream of the throat varies the nozzle internal expansion area ratio as required over a range of operating pressure ratios.

The arrangement of the ADEN nozzle flaps, expansion ramp, actuators, and structural elements has been chosen carefully to allow smooth afterbody contours. The nonaxisymmetric nozzle shape blends well with supersonic airframe lines minimizing drag producing base regions, and the cruise throat aspect ratio, 4×1, permits the ADEN to be installed without increasing frontal projected area. For V/STOL operation, a rotating deflector mounted outside the nozzle casing diverts the jet downward.

An additional feature of the ADEN is the capability to provide in-flight thrust vector control to improve aircraft flight maneuver capabilities by utilizing a variable external expansion ramp (VEER). The VEER upper surface is designed to blend with the airframe contours and the inner surface is contoured for effective jet expansion control. Variation of the VEER angle will deliver an upward or downward vertical thrust component as desired.

III. Test Arrangement and Model Description

The test program was conducted in the the 16 ft Propulsion Wind Tunnel at the Arnold Engineering Development Center. The test article was a 1/8th scale model of a Grumman-designed twin engine, thrust vectoring, V/STOL fighter. As shown in Fig. 2, the overall model was supported by a bifurcated twin boom system that attached to the model vertical tails. The high-pressure air supply for powering the model and all instrumentation lines were housed within this support system.

The model force balance arrangement is illustrated in Fig. 3. With the exception of the vertical tails, the entire model was fully metric to a six-component flow-through aircraft main balance. This balance measured total aircraft forces and moments. The main balance metric break was located at the base of the vertical tails. In addition, a second six-component balance, "piggy-backed" onto the main balance, was employed to measure forces and moments on the left-hand nozzle. At wind-on conditions, this auxiliary balance was used merely as a diagnostic. Because the influence of the jet exhaust feeds upstream of the nozzle balance metric system, the main balance must be employed for all lift/drag comparisons to ensure the accounting of all jet-induced phenomena.

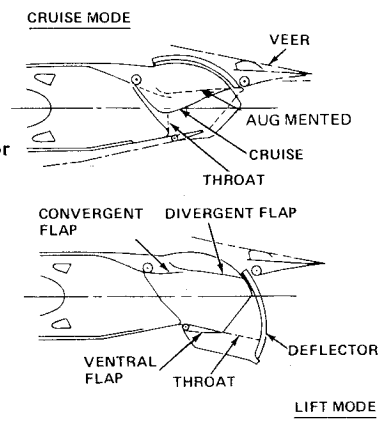

Fig. 1 Augmented deflector exhaust nozzle.

Presented as Paper 78-1080 at the AIAA/SAE 14th Joint Propulsion Conference, Las Vegas, Nev., July 25-27, 1978; submitted Nov. 14, 1978; revision received April 2, 1979.

Index categories: Airbreathing Propulsion; Aerodynamics.

*Propulsion Project Engineer.
†Corporate Group Head, Fluid Mechanics.

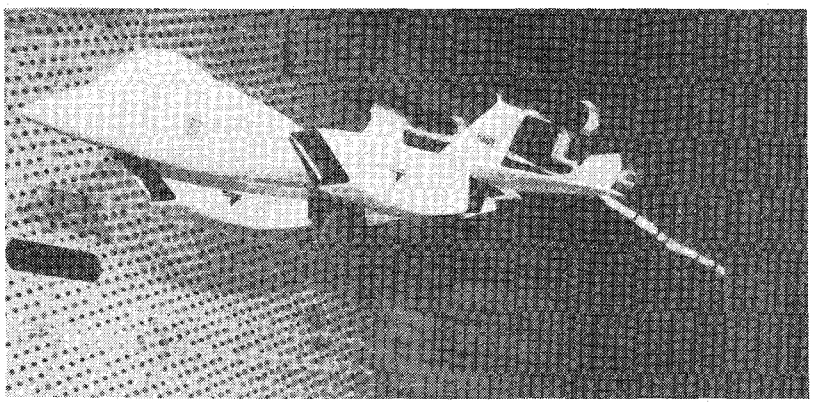

Fig. 2 Model in 16-ft AEDC wind tunnel.

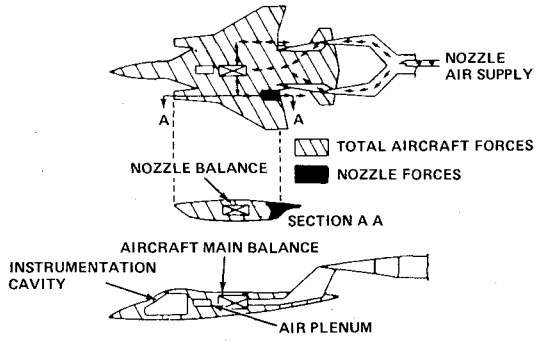

Fig. 3 Force balance arrangement.

IV. Test Program and Procedures

In this program, the ADEN and ALBEN nonaxisymmetric nozzles and a circular convergent-divergent axisymmetric nozzle were evaluated. A previous publication[3] discussed the results of the nonafterburning unvectored ADEN and ALBEN compared to the circular baseline nozzle. This paper will concentrate on the study of the vectoring ADEN which was evaluated over a range of geometric deflection angles at both maximum and nonafterburning conditions. Figure 4 presents photographs comparing the extremes in VEER deflection that were tested.

Mach number was varied from 0.6 to 1.5; however, the heaviest emphasis was placed on the 0.6-0.9 range because that is the regime where the largest drag reductions due to vectoring were anticipated. Angle of attack was varied from -1 to $+11$ deg depending on Mach number. The high-pressure air supply was used to simulate nozzle pressure ratios from 1.25 to 10.0. In addition, jet-off data were taken at each Mach number and angle of attack as a reference condition to which the power-on data could be compared.

All configurations were intentionally tested without horizontal tails so that the thrust vectoring results could be applied to a canard-type or horizontal-tail-type aircraft by adding an appropriate correction to the test data.

The test technique employed in this program used a thrust-measuring device, however, the desired parameters were thrust-removed coefficients (e.g., drag). Thus, the static internal thrust components had to be removed from the corresponding wind-on components that included direct thrust forces (i.e., thrust minus drag). In order to minimize the error associated with this subtraction of two large numbers, the static thrust measurements were obtained during the same "model-build" as employed for the wind-on tests.

The basic measurement objective of this test was to obtain total aircraft drag, lift, and pitching moment. In order to be completely meaningful, these parameters must include the installation effects of the thrust vector, but not the magnitude of the uninstalled thrust vector itself.

Ultimately, blown model data are combined with real engine data so that full-scale aircraft performance can be predicted. Real engine data are always provided in terms of static uninstalled thrust at the static uninstalled vector angle. Therefore, as a matter of practicality, the model total lift and drag data must be presented in the same format, i.e., based on the removal of static thrust at the static vector angle (as opposed to wind-on thrust at the wind-on vector angle) from the wind-on thrust minus drag. Hence, the term "thrust-removed parameter" was originated (e.g., thrust-removed drag, $C_{D_{TR}}$).

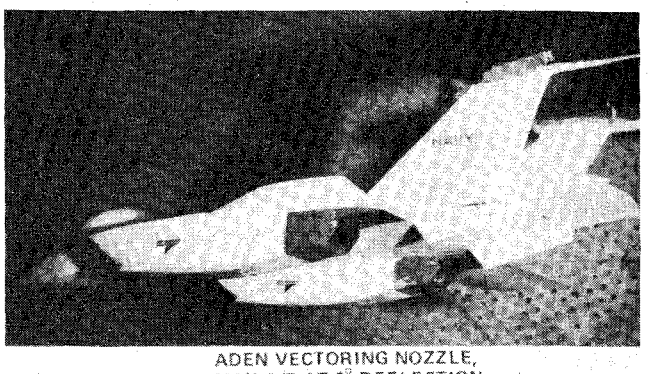

ADEN VECTORING NOZZLE,
MAX-A/B AT 0° DEFLECTION

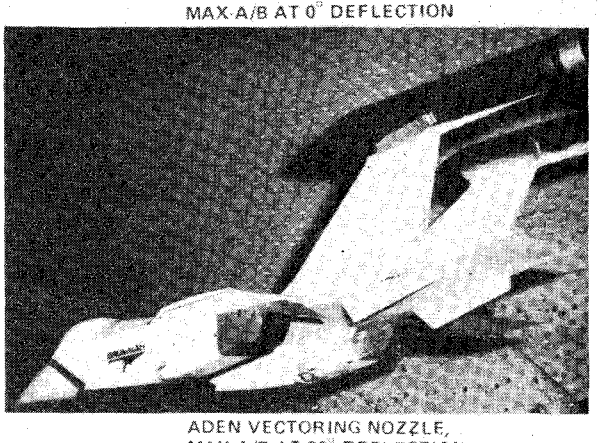

ADEN VECTORING NOZZLE,
MAX-A/B AT 20° DEFLECTION

Fig. 4 Representative nozzles mounted in model.

V. Static Test Results

The axial thrust characteristics for the vectoring ADEN in the cruise mode are shown in Fig. 5a. These nonaxisymmetric nozzle performance curves exhibit two "peaks," typical for internal/external expansion nozzles, occurring at nozzle pressure ratios associated with the internal and external area ratios. As expected, the performance drops off as the VEER is rotated downward. This decrease is due to supersonic flow turning which causes shock waves to develop and a reduction of the effective overall area ratio. The result is a loss of exit momentum. A negative VEER rotation may produce better performance.

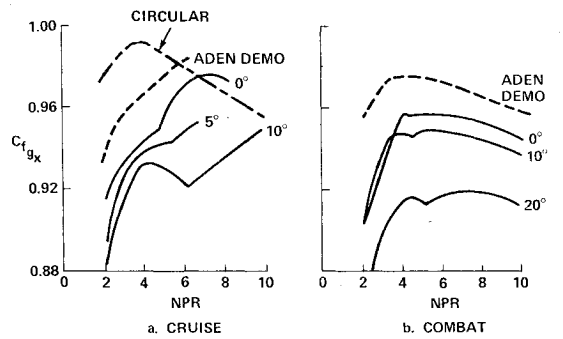

Fig. 5 Axial static performance for all ADEN models.

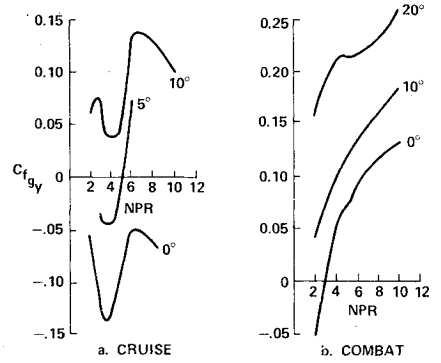

Fig. 6 Vertical static performance for all ADEN models.

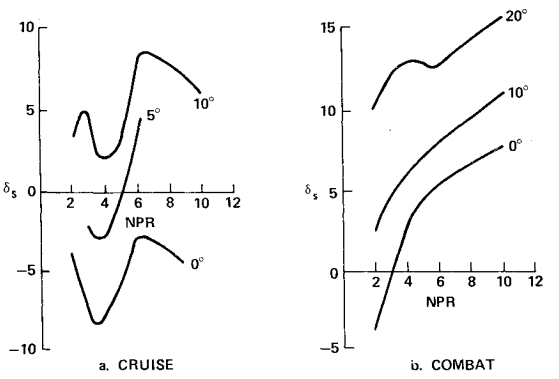

Fig. 7 Static thrust vector angle for all ADEN models.

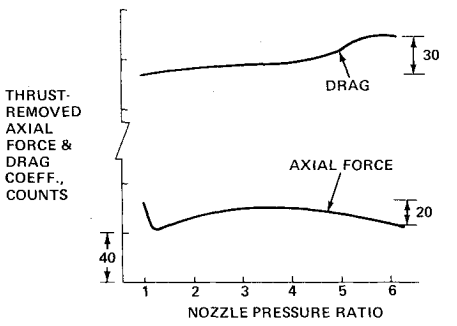

Fig. 8 Axial force and drag comparison.

For comparison, the unvectored circular nozzle static thrust characteristic is also shown in Fig. 5a. At a pressure ratio for cruise, NPR = 6.0, the ADEN cruise 0 deg nozzle tested has an internal performance value approximately 0.8% lower than the circular nozzle. Independent static peformance testing was performed by the General Electric Company[4] to develop the final ADEN design subsequent to the fabrication of the test nozzles discussed in this paper. This final design (ADEN Demo) incorporated a short VEER and a modified divergent flap contour. An axial thrust coefficient improvement of about 2% over the ADEN cruise 0-deg nozzle reported in this paper was obtained. The performance of the ADEN Demo is presented as a dashed line in Fig. 5. This curve shows that an ADEN is competitive with a circular nozzle from an internal performance standpoint for the cruise NPR designated.

The axial static performance characteristics for the ADEN combat nozzle are shown in Fig. 5b. The overall trends are similar to those of the cruise nozzle in that: 1) the double peak phenomenon is apparent, and 2) performance falls off at high-deflection angles. However, the combat nozzle flowpath is different from that of the cruise nozzle, and it is possible that its VEER setting for optimum static performance may be between 0 and 10 deg, rather than the negative angle that is postulated for the cruise nozzle. Note that the ADEN Demo, in the combat mode, also produces aproximately 2% static performance improvement over the ADEN tested in this program.

Figure 6 compares the vectored and unvectored ADEN test nozzle vertical thrust coefficient data. The ADEN cruise nozzle curve shapes for the vectored configurations are very similar to those for unvectored cruise configuration. The vertical thrust coefficient increment between curves is very nearly constant as NPR is varied and its value appears to be in direct comparison to the VEER deflection angle. The ADEN combat vertical thrust coefficient curves show similar, but not as pronounced, trends. The total flowpath turning angle is not as great for the combat nozzles as it is for the cruise nozzles and, therefore the "roller coaster" effect for the vertical thrust coefficient is not seen here until the VEER deflection approaches 20 deg.

The thrust vector angle data for ADEN vectored and unvectored test nozzles are presented in Fig. 7. This figure illustrates the vector angle sensitivity to NPR and VEER position. Note that the vector angle trend with NPR closely corresponds, as expected, to the vertical thrust coefficient trend. The thrust vector variations with NPR are caused by the asymmetric flowpath. This results in unbalanced pressure forces which vary with NPR and VEER setting. Thus, the measured thrust vector angle is actually the effective direction of the force produced by a combination of exit momentum and a pressure area force felt by the divergent flap and VEER expansion surfaces. The static vector angle will be altered by the external flow at wind-on conditions.

VI. Wind-On Test Results

This section displays all major model test results for the ADEN family of nozzle configurations at wind-on conditions. All results are presented in terms of thrust-removed parameters.

Effect of Power on Drag/Lift Components

Historically, when studying axisymmetric nozzle installations, such as the F-14[5] and other current state-of-the-art aircraft, the jet effects (jet-on minus jet-off increment) on axial force and drag were indistinguishable. For the asymmetric ADEN configuration, very dramatic differences exist between the jet effects on axial force and drag, as shown in Fig. 8. The results are for the unvectored ADEN curise 0 deg configuration at Mach 0.8 and $\alpha = 8$ deg. The axial force trend with NPR exhibits the classical S-shaped curve, but the drag trend is totally different. The jet-effects increment at NPR = 6.0 is a negative (favorable) 20 counts for axial force and a positive (unfavorable) 30 counts for drags. For conventional axisymmetric installations these two jet-effects increments would be identical. It is clear that the ADEN nonaxisymmetric nozzle even when unvectored exhibits complex characteristics that require a greater level of understanding than has been traditionally employed.

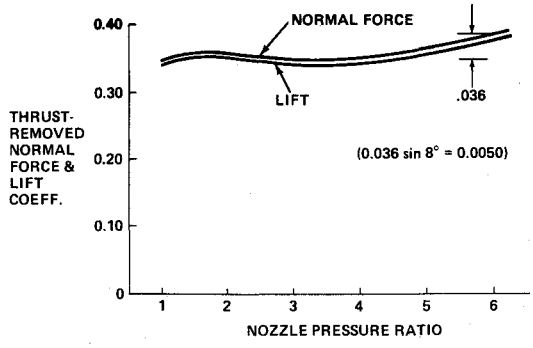

Fig. 9 Normal force and lift comparison.

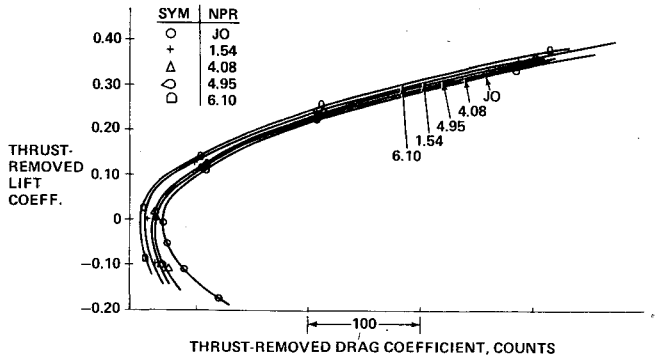

Fig. 10 Effect of power on drag polar, ADEN CR 0 deg, Mach 0.8.

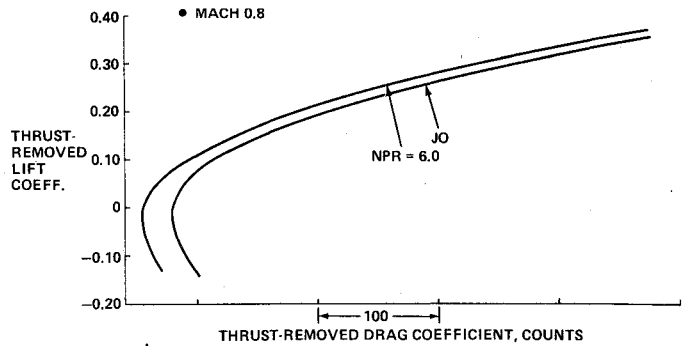

Fig. 11 Effect of power on drag polar, circular nozzle.

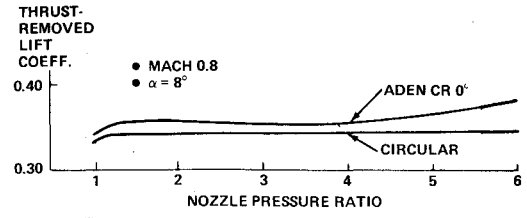

Fig. 12 Effect of power on aircraft lift.

The explanation of these different trends appears in Fig. 9, which shows that normal force and lift are sensitive to power. As expected, normal force and lift have virtually the same shape becuase axial force has only a third-order effect on lift at this angle of attack. As noted in Fig. 9, a 0.036 change in normal force coefficient creates a 50 count impact on drag. This more than offsets the −20 count (Fig. 8) axial force contribution to drag to result in a net 30 count jet effects drag increment. Because both lift and drag components are power-sensitive, the drag polar must be the figure of merit in judging the total effects of power.

Under vectored conditions,the ADEN cruise configuration exhibits the same drag and lift trends; however, these trends are much more dramatic due to increased flowfield asymmetry relative to the wing chord plane. For example, the jet-effects increments noted previously are two to three times greater for the ADEN cruise 10 deg configuration.

Effect of Power on Aircraft Drag Polar

The effect of power on the untrimmed aircraft drag polar of the wing-mounted ADEN installation is significantly different from that obtained with either circular aft-mounted or circular wing-mounted installations. Figure 10 presents the ADEN configuration drag polars at several power conditions relative to the jet-off condition. All the power-on polars are significantly more favorable than the power-off polar. At an NPR equal to 4.95 (which is a reasonable operating NPR at Mach 0.8), the jet-effects increment varies from 18 counts at zero lift to 44 counts at a $C_{L_{TR}}$ equal to 0.35. Thus, this power increment is highly dependent upon lift. The additional 26-count favorable power effect at a cruise lift condition relative to zero lift is due to reduced drag, which results from achieving the same $C_{L_{TR}}$ at a lower angle of attack. This is a clear example of favorable jet/wing interaction.

Conventional aft-mounted circular installations (e.g., F-14 and F-15) do not exhibit such variations in the jet-effects increment, mainly because there is no lifting surface for the jet exhaust to act upon. On the other hand, a wing-mounted circular installation might be expected to develop some jet/wing interactions. However, for this configuration it is minimal, as shown in Fig. 11. At zero lift, the power increment, which is favorable, is about 25 counts; at a $C_{L_{TR}}$ equal to 0.35, this increment has increased only slightly to about 30 counts. Obviously, the reason why the jet-effects increment of the circular wing-mounted installation does not exhibit any significant synergistic improvements as C_L increases, is because the circular nozzle does not integrate effectively with the wing. It, therefore, cannot generate significant jet-induced lift as does the ADEN installation.

Figure 12 explains why the drag polar of the ADEN configuration, even when unvectored, exhibits favorable jet/wing interactions which are not characteristic of the circular installation. Once the circular nozzle jet exhaust is on, this installation shows virtually no change in lift coefficient. This means that drag coefficient changes due to NPR from one jet-on condition to another must necessarily be independent of lift. It is only from jet-off to a nominal flow through NPR (i.e., 1.5) that a slight effect is observed. On the other hand, the ADEN exhibits a significant increase in lift at operating NPRs relative to jet-off conditions. Thus, it is these differences in lift characteristics between the two installations that cause significant polar rotations for the ADEN, while the circular installation polars exhibit virtually no rotation as NPR increases.

Because the ADEN polars rotate instead of translate as power is increased, aero/propulsion bookkeeping procedures will be more complicated for the ADEN than either aft-mounted or wing-mounted circular installations. Thus, even for the ADEN in its unvectored mode, a more thorough testing procedure is required than has been employed for conventional axisymmetric installations. Jet effects must now be investigated over the complete lift range, not just at $\alpha = 0$ deg for example. In summary:

(ΔC_D) power $= f$(NPR)	Conventional axisymmetric
(ΔC_D) power $= f$(NPR, C_L)	ADEN/wing-mounted

Effect of Vectoring on Lift

Vectoring the ADEN results in substantial increases in the thrust-removed aircraft lift coefficient. Figure 13 shows how the aircraft lift (aerodynamic lift plus jet-induced lift) increases as the geometric deflection angle is increased at a typical Mach 0.9 operating condition.

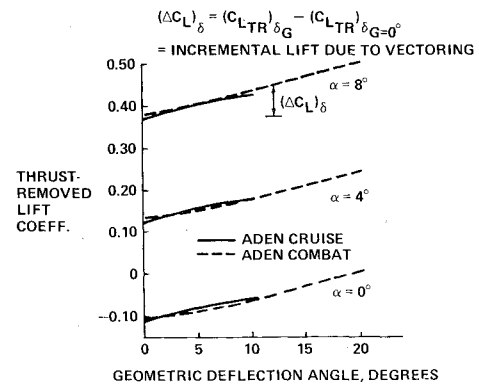

Fig. 13 Effect of ADEN vectoring on aircraft lift, Mach 0.9, NPR = 4.95.

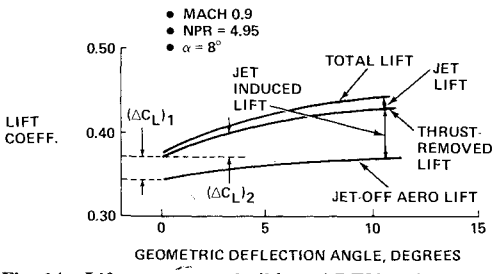

Fig. 14 Lift-component buildup, ADEN cruise nozzle.

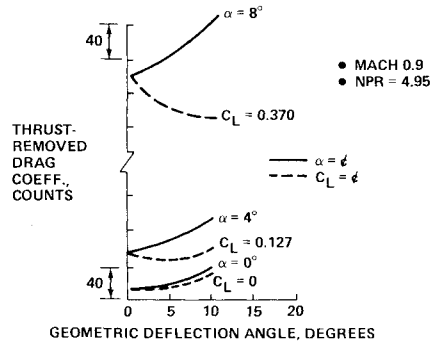

Fig. 15 Effect of vectoring on aircraft drag, ADEN cruise nozzle.

It is instructive to analyze the three contributors that comprise the total nozzle/airframe lift. The lift-component buildup is illustrated for the ADEN cruise configuration at a typical Mach 0.9 operating condition in Fig. 14. The jet-off aerodynamic lift is the foundation for the buildup and represents only aerodynamic effects without any influences form the propulsion system (other than the presence of the nozzle). The second component in the buildup is the propulsive jet-induced lift which, when added to the basic aero lift, yields the thrust-removed lift due to the propulsion system relative to uninstalled conditions. When the direct jet lift is added to the thrust-removed lift, the total lift is obtained. This direct jet lift $C_\mu \sin(\alpha+\delta_s)$ is the geometrical component of the resultant gross thrust vector in the lift direction.

Effect of Vectoring on Drag

The lift enhancement benefit generated by thrust vectoring at constant angle of attack does not come without a penalty. Figure 15 shows that an increase in ADEN cruise nozzle deflection angle is accompanied by a sizable drag production (at constant angle of attack). Note that the rate at which drag increases with jet deflection is strongly dependent on angle-of-attack magnitude, as expected. The same trends also apply to the ADEN combat configuration.

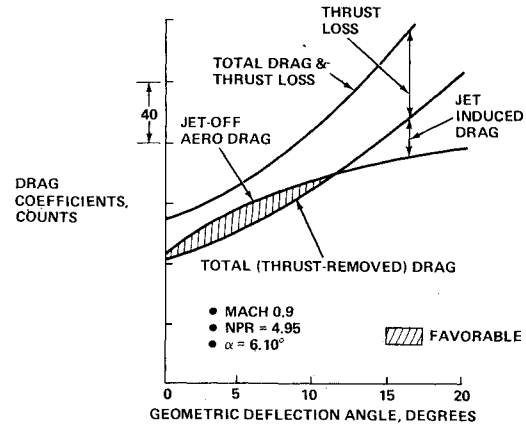

Fig. 16 Drag-component buildup, ADEN combat nozzle.

Figure 15 also provides a comparison for studying drag variations due to vectoring with a constant α or constant C_L format. Major differences exist between the two formats and these differences are dependent on the magnitude of α and/or C_L. At $\alpha = 0$ deg, when drag equals axial force, and at $C_L = 0$, when normal force is very small, the two presentation formats are very similar in that the drag trends with deflection are roughly the same. At conditions where substantial differences exist between drag and axial force and when normal force is not small, the two formats yield very different results. Furthermore, the disparity increases as the magnitude of α and/or C_L increases.

No conclusions can be made about the aircraft sensitivity to thrust vectoring if one only had the constant α characteristics. The constant C_L format has more significance because definite conclusions can be made about the aircraft polars. For example:

1) At moderate lifting conditions ($C_{L_{TR}} = 0.127$), the drag polars become favorable as vector angle increases from a 0 deg to about a 5 deg deflection angle, then unfavorable as it increases to a 10 deg deflection angle.

2) At higher lifting conditions ($C_{L_{TR}} = 0.370$), the drag polars are always more favorable as vector angle is increased from 0 to 10 deg deflection angles.

Excluding trim drag and ram drag components, which will be discussed later, the buildup of forces in the drag direction is composed of three elements: 1) jet-off aerodynamic drag, 2) propulsion jet-induced drag, and 3) thrust-loss. The jet-off aerodynamic drag includes no propulsion system effects. The propulsion jet-induced drag is the jet-effect increment caused by the influence or the nozzle efflux. These two components when added together form the total thrust-removed drag which includes all nozzle installation effects. The thrust loss, $C_\mu[1-\cos(\alpha+\delta_s)]$, is the geometrical component of the uninstalled gross thrust vector resolved along the wind axis.

The drag component buildup at a typical Mach 0.9 operating condition for the ADEN combat configuration at a constant angle of attack, shown in Fig. 16, is characterized by an interesting feature. The jet-induced drag is favorable (negative) in the 0-11 deg deflection angle range. This partially, but not completely, offsets the thrust loss penalty. It is not uncommon to have such a favorable jet-induced drag for it is caused by the interplay between jet-induced axial force (a negative number) and jet-induced normal force (a positive number), which vary in magnitude with deflection angle.

Effect of Vectoring on Aircraft Drag Polar

In this section the individual lift and drag components discussed earlier are combined to form the aircraft polars for different vectoring conditions. The drag polar data presentation format must be used to study the effects of thrust vectoring. This is because lift as well as drag is nozzle dependent for the ADEN installation.

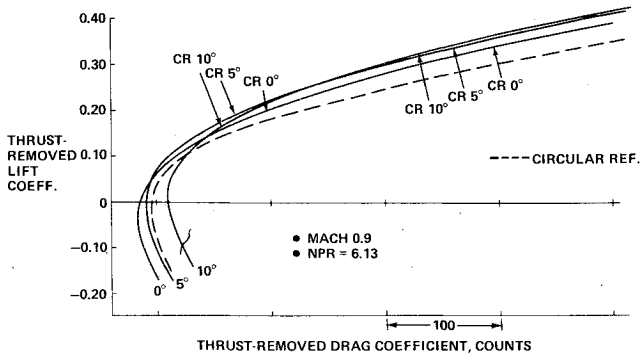

Fig. 17 Effect of vectoring on thrust-removed polars, ADEN cruise nozzle.

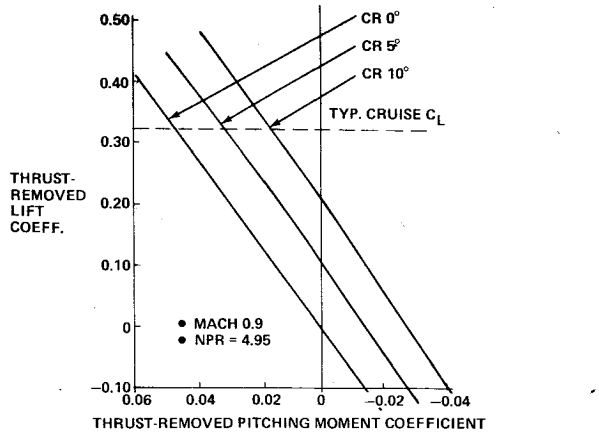

Fig. 18 Effect of thrust-vectoring on pitching moment, ADEN cruise nozzle.

The cruise nozzle polars at a typical Mach 0.9 condition for each vectoring mode are compared in Fig. 17. Also shown in the figure, for reference purposes, is the circular installation drag polar. Note the three distinct regimes for the ADEN configuration. At negative values of lift, the best-to-worst trend is 0, 5, 10 deg. In other words, vectoring increases drag at this "nonreal world" condition. At moderate values of lift, the best-to-worst trend is either 5, 0, 10 deg or 5, 10, 0 deg. In either case, an optimum deflection angle somewhere between 0 and 10 deg must exist. At higher values of lift, the best-to-worst trend is 10, 5, 0 deg, which is the reverse of the negative lift trend.

In this case, three vectoring angles were evaluated and three separate regimes for the polars were observed. One can generalize and say that if there were four configurations tested, then four regimes would have been observed, and so on. As higher C_L regimes are entered, it is always a larger deflection angle that will be the optimum. This should be true up to the point where the supercirculation flowfield breaks down (just as a wing flowfield breaks down at high angles of attack). An optimum polar locus, composed of an envelope of points covering a range of deflection angles, can therefore be envisioned. This indicates that deflection angle should be scheduled to angle of attack to achieve optimum performance.

The magnitude of the drag reduction due to vectoring is significant. This can be observed by entering the polar at a constant $C_{L_{TR}}$ (0.35, for example). Vectoring 5 deg results in a 34 drag count reduction, while vectoring 10 deg yields a 41 drag count reduction relative to 0 deg. Vectoring the second 5 deg, a 100% increase, results in only an additional 20% drag improvement. This suggests that large amounts of vectoring are not necessary to show substantial payoffs.

A word of caution is warranted. The preceding discussion applies to the untrimmed thrust-removed polars obtained from the model. From the point of view of nozzle/airframe aerodynamics, these polars can be very useful in judging the relative trends of thrust vectoring. However, four items are missing to complete the aircraft performance analysis: 1) jet lift, 2) thrust-loss, 3)trim drag, and 4) ram drag.

Effect of Vectoring on Pitching Moment

The untrimmed polar improvements due to vectoring the ADEN must be adjusted for trim effects. For example, if vectoring resulted in a larger trim drag requirement, then some of the untrimmed polar benefit would be reduced. Conversely, if vectoring reduced the trim penalty, then the untrimmed polar benefit would be increased further. For the specially designed V/STOL configuation tested in this program, the latter case is applicable, as will be discussed.

Figure 18 shows the effect of vectoring the ADEN cruise nozzle on aircraft tail-off pitching moment. These Mach 0.9 results, which indicate an unstable situation ($dC_M/dC_L > 0$), are representative of the trends obtained throughout the 0.6-0.9 Mach range. It is noted that this airplane configuration was intentionally designed to be statically unstable (with tail on) at subsonic speeds, because fly-by-wire technology was employed to minimize trim penalties relative to those of a statically stable configuration.

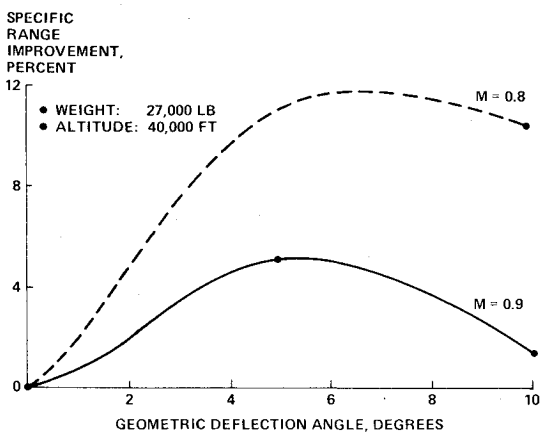

Fig. 19 Effect of vectoring on specific range, ADEN cruise nozzle.

The figure demonstrates the effect of cruise nozzle vectoring at subsonic conditions. At conditions of interest as geometric deflection angle is increased, the pitching moment needed to be trimmed-out decreases. For example, at a typical cruise 0.32 $C_{L_{TR}}$, the 10 deg nozzle produces a 0.03 pitching moment improvement relative to the 0 deg nozzle. Thus, it is concluded that vectoring the ADEN at conditions of interest is favorable for trim, and aircraft performance improvements are actually in excess of those indicated by the untrimmed polars of Fig. 17.

Similar trends were obtained for the ADEN combat nozzle and, at a typical 0.60 maneuver C_L, increases in deflection angle from 0 to 20 deg result in progressive reductions in trim required.

VII. Application of Model Results to Aircraft Performance

This section shows how the scale model, thrust-removed data are combined with real engine uninstalled data to obtain aircraft performance. This will be done for subsonic cruise and combat maneuver conditions in order to study the payoffs of thrust vectoring. In addition the subsonic cruise mission results will be compared to the baseline circular C-D nozzle.

Table 1 Summary output for cruise mission analysis

δ_G, deg	$C_{L_{reqd}}$	α, deg	NPR	C_μ	W_{fuel}, lb/h	$\Delta R/R$, %
0	0.400	8.45	5.22	0.0973	2210	0
10	0.400	7.16	4.93	0.0888	2000	10.5

Table 2 Specific range analysis for circular nozzle installation

Configuration	δ_G, deg	$C_{L_{reqd}}$	α, deg	NPR	C_μ	W_{fuel}, lb/h	$\Delta R/R$, %
Circular	4	0.400	8.64	5.45	0.1024	2410	0
ADEN CR, 0 deg	0	0.400	8.45	5.22	0.0973	2210	9.0

Vectoring Payoffs at Subsonic Cruise

The cruise mission analysis is illustrated at Mach 0.8 and 40,000 ft for the ADEN cruise 0 and 10 deg configurations, both of which will then be compared to a baseline circular installation. Preliminary aerodynamic parametric studies have shown that this Mach number and altitude are close to optimum for this airplane design. A 27,000 lb weight was selected for the analysis because it represents about a 50% fuel weight for this airplane. To be conservative, no credit was taken for the favorable trim characteristics of the ADEN cruise 10 deg relative to the cruise 0 deg configuration.

The steady-state equilibrium equations in lift and drag directions are solved with the test data relationships using iterative methods by employing guesses of both α and NPR. Once these two independent variables are found, all the dependent variables (e.g., C_L, and C_D) can readily be obtained. In addition, the fuel flow, W_{fuel}, and the incremental specific range, ΔR, are easily determined using full-scale data.

A summary output for the cruise mission analysis is shown in Table 1. Several items in the Table 1 are noteworthy.

1) Vectoring 10 deg allows for a 15% reduction (1.3 deg) in α, while still maintaining the same required lift ($C_{L_{reqd}} = 0.400$).

2) The reduced angle of attack results in lower drag leading to almost a 9% reduction in resultant gross thrust coefficient (C_μ).

3) This reduced power (NPR) level translates into a 10.5% savings in fuel and a corresponding 10.5% increase in specific range.

The same analysis was repeated at Mach 0.9, with all other ground rules the same. At this Mach number, the ADEN cruise 5 deg configuration was evaluated in addition to the cruise 0 and 10 deg. Figure 19 presents the incremental specific range improvement as a function of deflection angle for both Mach conditions. Note that for the Mach 0.9 case, an optimum deflection angle is clearly indicated. Based on this trend, the Mach 0.8 characteristic has been conservatively faired. At an optimum angle, approximately equal to 7 deg, the payoff in specific range is about 12%. This is a very significant improvement to aircraft cruise performance.

The cruise specific range analysis described previously was also applied to the circular nozzle installation at Mach 0.8 to obtain an aircraft performance comparison between the unvectored ADEN and the baseline circular nozzle. The results of the specific range analysis for the circular installation are summarized in Table 2 and are compared with the ADEN cruise 0 deg configuration. Relative to the circular baseline, the unvectored ADEN cruise 0 deg installation features a 9.0% increase in specific range. This is a very significant improvement to aircraft cruise performance.

The total payoff for the vectoring ADEN relative to the circular baseline is obtained by combining this result with the results for the optimum ADEN deflection angle of 7 deg, as shown in Fig. 19. This is presented in the bar chart of Fig. 20. The 9.0% drag cleanup payoff when added to the 12.0% ADEN vectoring payoff yields a total ADEN cruise specific range payoff of 21%.

Table 3 Summary output for sustained maneuver analysis

δ_G, deg	NPR	C_μ	α, deg	$\Delta g/g$, %
0	5.79	0.1438	10.47	0
10	5.79	0.1435	9.95	5
20	5.79	0.1408	8.90	6

Vectoring Payoff at Combat Maneuver

In addition to the ADEN installation payoff at cruise, it is also possible to derive performance payoffs at sustained (max-A/B) maneuver conditions. The combat 0, 10, and 20 deg model results are matched with the engine data, as will be discussed.

The maneuver analysis is conducted at a typical Mach 0.9, 20,000 ft condition using the same 27,000 lb airplane weight. Again, to be conservative, no credit is taken for the favorable trim effect of vectoring. A summary output for the sustained maneuver analysis is given in Table 3.

When vectoring from 0 to 20 deg, a 6% improvement in g-capability is achieved. Figure 21 shows the complete payoff in terms of percent improvement in g-capability as the ADEN is vectored from 0 to 20 deg. Observe that at an optimum deflection angle of about 17 deg, greater than 6% improvement in sustained maneuver capability is achieved relative to the unvectored configuration. This improvement can be utilized either to enhance an airplane's dog-fight capability or to resize the wing to reduce takeoff gross weight (TOGW) while maintaining the same maneuver capability.

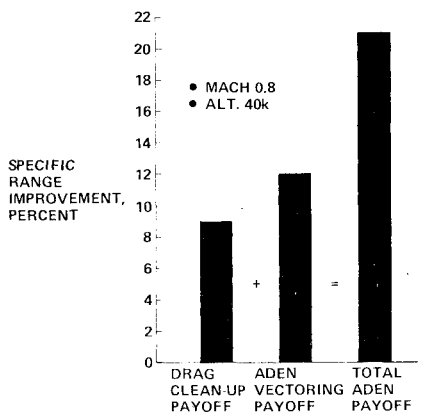

Fig. 20 ADEN cruise performance payoffs relative to circular baseline installation.

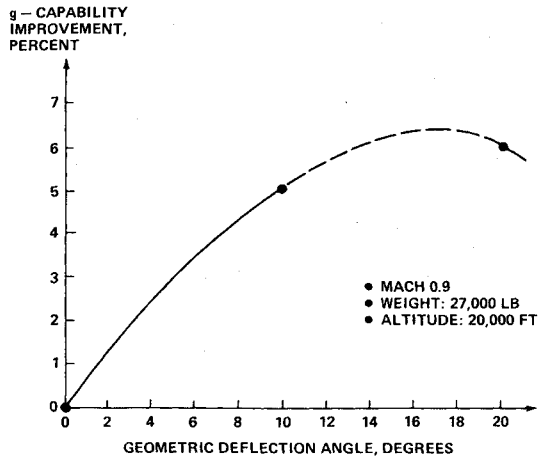

Fig. 21 Effect of vectoring on *g*-capability, ADEN combat nozzle.

VIII. Conclusions

The overall test program produced a large number of significant conclusions. The following is a list of the most noteworthy conclusions:

1) A fully metric model is necessary for lift-enhancement investigations, because jet-induced supercirculation is not a localized phenomenon.

2) Unvectored nonaxisymmetric nozzle static thrust performance levels can be made competitive with axisymmetric nozzles.

3) For nonaxisymmetric wing-mounted nozzle installations, drag does not correlate with power in the traditional fashion because lift, as well as drag, is power sensitive. On the other hand, axial force does correlate with power in the usual sense for both the vectored and unvectored ADEN.

4) The effect of increases in power on the ADEN drag polar is to produce a favorable rotation caused by the lift-sensitive power effect as angle of attack is increased.

5) For either vectored or unvectored modes, different drag trends occur when ADEN power is varied at constant lift compared to constant angle of attack.

6) For this ADEN installation supercirculation lift, resulting from power effects, is achieved even in the undeflected mode. This is then augmented by a second component of supercirculation lift caused by vectoring a given mass flow.

7) Vectoring the ADEN has a dramatic effect on polar shape. An optimum polar locus is formed by an envelope of points covering a range of deflection angles. This means that deflection angle should be scheduled to angle of attack to achieve optimum performance.

8) Relative to undeflected conditions, non-A/B and max-A/B vectoring modes both exhibit lower trim drag at conditions of interest, which will further increase the performance benefits noted previously.

9) When evaluating nonaxisymmetric nozzle test data, the trimmed drag polar, as opposed to drag component curves, must be used as the figure of merit.

10) Signficant performance gains are realized when the nonaxisymmetric nozzles are vectored. At a representative Mach 0.8 dry power cruise condition, a 12% specific range improvement is achieved when the ADEN is vectored at the optimum 7 deg geometric deflection angle.

11) When the unvectored drag cleanup payoff (nonaxi- compared with axi-) is combined with the vectoring payoff, a 21% specific range improvement is achieved for the vectored nonaxisymmetric nozzle installation.

12) At Mach 0.9, 20,000 ft, greater than a 6% improvement in sustained (maximum power) maneuver capability is achieved at a 17 deg optimum geometric deflection angle, compared to the unvectored nonaxisymmetric nozzle configuration.

Acknowledgment

The authors wish to acknowledge the technical assistance provided by J.A. Laughrey and G.K. Richey of AFFDL/FXM; D.C. Baker and T.L. Kenedy of ARO, Inc.; J.L. Palcza of Naval Air Propulsion Test Center; G.E. Hoff of General Electric; and W.J. McAllister, R.E. Krepski, and K. Lango of Grumman Aerospace.

References

[1] Richey, G.K., Berrier, B.L., and Palcza, J.L., "Two-Dimensional Nozzle/Airframe Integration Technology—An Overview," AIAA Paper 77-839, Orlando, Fla., July 1977.

[2] Berrier, B.L., Palcza, J.L., and Richey, G.K., "Nonaxisymmetric Nozzle Technology Program—An Overview," AIAA Paper 77-1225, Seattle, Wash., Aug. 1977.

[3] Schnell, W.C. and Grossman, R.L., "Wind Tunnel Test of a Propulsive Lift Enhancement Model," AFFDL-TR-78-104, Aug. 1978.

[4] Boardman, W.R., "Augmented Deflector Exhaust Nozzle (ADEN) Demonstrator 1/8 Scale Cold Flow Static Test Results," General Electric Rept. R75 AEG-301, Sept. 1975.

[5] Schnell, W.C., "F-14 Installed Nozzle Performance," AIAA Paper 77-1225, San Diego, Calif., 1974.